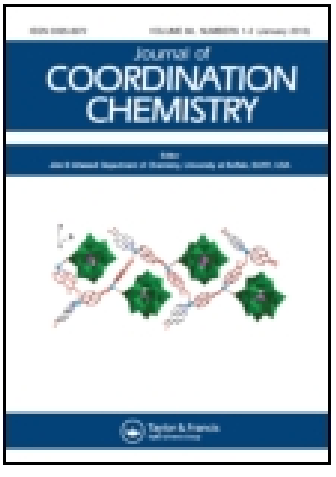

Journal of Coordination Chemistry
Publication details, including instructions for authors and subscription information:
http://www.tandfonline.com/loi/gcoo20

A 2-D organic-inorganic supramolecular layer based on a $\{P_2Mo_5\}$ cluster bridged by Mn(II) and pentanuclear fragment linker

Jie Shi[ab], Chunxiao Wang[ab], Kai Yu[ab], Zhanhua Su[ab], Chunmei Wang[ab] & Baibin Zhou[ab]

[a] Key Laboratory for Photonic and Electronic Bandgap Materials, Ministry of Education, School of Chemistry and Chemical Engineering, Harbin Normal University, Harbin, PR China

[b] Key Laboratory of Synthesis of Functional Materials and Green Catalysis, Colleges of Heilongjiang Province, Harbin Normal University, Harbin, PR China

Accepted author version posted online: 18 Jul 2014.Published online: 11 Aug 2014.

To cite this article: Jie Shi, Chunxiao Wang, Kai Yu, Zhanhua Su, Chunmei Wang & Baibin Zhou (2014) A 2-D organic-inorganic supramolecular layer based on a $\{P_2Mo_5\}$ cluster bridged by Mn(II) and pentanuclear fragment linker, Journal of Coordination Chemistry, 67:13, 2229-2237, DOI: 10.1080/00958972.2014.946414

To link to this article: http://dx.doi.org/10.1080/00958972.2014.946414

Journal of Coordination Chemistry, 2014
Vol. 67, No. 13, 2229–2237, http://dx.doi.org/10.1080/00958972.2014.946414

A 2-D organic–inorganic supramolecular layer based on a $\{P_2Mo_5\}$ cluster bridged by Mn(II) and pentanuclear fragment linker

JIE SHI†‡, CHUNXIAO WANG†‡, KAI YU*†‡, ZHANHUA SU†‡, CHUNMEI WANG†‡ and BAIBIN ZHOU*†‡

†Key Laboratory for Photonic and Electronic Bandgap Materials, Ministry of Education, School of Chemistry and Chemical Engineering, Harbin Normal University, Harbin, PR China
‡Key Laboratory of Synthesis of Functional Materials and Green Catalysis, Colleges of Heilongjiang Province, Harbin Normal University, Harbin, PR China

(*Received 4 May 2014; accepted 13 June 2014*)

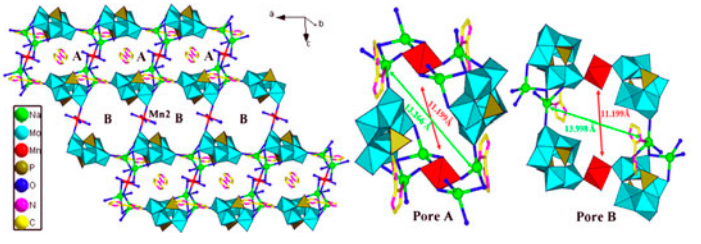

Mn^{2+} and unusual pentanuclear fragments $\{[Na_{0.5}(H_2O)_{0.5}]_2Mn(OH)_4(H_2O)_2[Na_{0.5}(H_2bim)]_2\}$ are introduced into $\{P_2Mo_5\}$ system to yield an infinite 2-D supramolecular layer with two cage-like pores. Compound **1** displays good electrocatalytic activity on reduction of hydrogen peroxide, and fluorescent properties in the solid state at room temperature.

An organic–inorganic hybrid based on $\{P_2Mo_5\}$ clusters, $(H_2bim)_3[\{Na_{0.5}(H_2O)_{0.5}\}_2\{Mn(OH)_4(H_2O)_2\}\{Na_{0.5}(H_2bim)\}_2\{Mn(H_2O)_4(P_2Mo_5O_{23})_2\}]\cdot 4H_2O$ (**1**) (bim = 2,2′-biimidazole), was hydrothermally synthesized and characterized by elemental analyses, IR, TG, UV, and single crystal X-ray diffraction analyses. In **1**, four Na ions, one Mn, and two bim ligands are linked by four μ–O bridges to form unusual pentanuclear fragments $[\{Na_{0.5}(H_2O)_{0.5}\}_2\{Mn(OH)_4(H_2O)_2\}\{Na_{0.5}(H_2bim)\}_2]$. Each pentanuclear segment links adjacent to four Standberg units to form supramolecular dimer chains, which are further connected by $Mn(H_2O)_4$ linkers to yield infinite 2-D layer. Two kinds of cage-like pores are observed in alternating type along the crystallographic *b* axis in which protonated H_2bim ligands fill one sort of pores. Electrochemical and fluorescent properties of **1** have been investigated.

Keywords: Hydrothermal synthesis; $[P_2Mo_5O_{23}]^{6-}$ polyanions; Electrochemistry; Fluorescent properties; Pentanuclear fragment

*Corresponding authors. Email: hlyukai188@163.com (K. Yu); zhou_bai_bin@163.com (B.B. Zhou)

1. Introduction

Synthesis of organic–inorganic hybrid materials has attracted interest due to their fascinating structural topologies and potential applications in catalysis, medicine, sorption, electrical conductivity, magnetism, and photochemistry [1–6]. An important strategy for the synthesis of POM hybrids is introduction of transition metal or transition metal complexes (TMCs), which can decorate and bridge, grafted into the framework of POM via covalent bonds [7–10] or weak intermolecular interaction. The introductions of the bridging units not only dramatically enrich the inorganic backbone, but also improve their chemical properties. New POM-based inorganic–organic hybrid compounds with 0-D, 1-D, 2-D, or 3-D frameworks have been reported [11, 12]. However, most of the POM-based compounds are modified by mononuclear TMCs or transition metals [13, 14]. Multinuclear segments decorating POM-based inorganic–organic hybrid compounds are less common. Thus, it would be a challenging but attractive area to synthesize this kind of compound.

Construction of POM-based multinuclear assemblies involves the selection and design of appropriate POM building blocks, organic ligands, and metal-connecting nodes [15]. As a unique class of metal oxide clusters, $[H_xMo_5P_2O_{23}]^{(6-x)-}$ (abbr. as P_2Mo_5; $x = 0, 1, 2$), has been regarded as suitable anionic templates to build up organic–inorganic hybrid structures. On one hand, the smaller size of polyanion leads to high negative charges of the whole clusters, which can induce more cationic linking units into the crystal structures and lead to plenty of structural topologies. On the other hand, the two extruding $\{PO_4\}$ fragments provide versatile coordination modes to various linking units. Moreover, the $\{P_2Mo_5\}$ clusters are easily available clusters that can be *in situ* synthesized with simple starting materials in routine synthesis or hydrothermal environment. Organic ligands play crucial roles in the construction of POM-based multinuclear hybrids because changes in the flexibility, length, and symmetry of the organic ligands can influence microstructure and character of hybrid materials. As a rigid organic ligand, 2,2′-biimidazole with four N-donors not only may coordinate with secondary metal to make frameworks robust but also have π-electron systems. Manganese ions have been widely used as the linking units to construct POM-based complexes due to their relatively strong coordination with both terminal oxygens of POMs and nitrogens of organic ligands [7–10]. Sodium ions usually act as the other type of linkers to construct POM-based assemblies, due to their more flexible coordination modes, low positive charge, and relatively high concentration in the starting materials. Recently, a series of compounds based on $\{P_2Mo_5\}$ modified by copper–H_2biim complexes were reported [16–19]. However, most studies are linked by transition metals, TMCs, or alkaline earth metals [20]; it is relatively rare that mixed pentanuclear metal fragments are linkers for construction of $\{P_2Mo_5\}$-based hybrids.

We report an inorganic–organic hybrid, $(H_2bim)_3[\{Na_{0.5}(H_2O)_{0.5}\}_2\{Mn(OH)_4(H_2O)_2\}\{Na_{0.5}(H_2bim)\}_2\{Mn(H_2O)_4(P_2Mo_5O_{23})_2\}]\cdot 4H_2O$, which is the first 2-D supramolecular layer based on $\{P_2Mo_5\}$ cluster bridged by Mn(II) and mixed-metal pentanuclear segments.

2. Experimental

2.1. *Materials and general procedures*

All reagents were purchased commercially and used without purification. Elemental analyses (C, H, N) were performed on a Perkin-Elmer 2400 CHN elemental analyzer.

P, Mo, Mn, and Na analyses were performed on a PLASMA-SPEC (I) inductively coupled plasma atomic emission spectrometer. IR spectra were obtained on an Alpha Centaurt FT/IR spectrometer with KBr pellets from 400 to 4000 cm^{-1}. The thermal gravimetric analyses were carried out in N_2 on a Perkin-Elmer DTA 1700 differential thermal analyzer with a heating rate of 10 °C min^{-1}. Diffuse reflectance UV–vis spectra ($BaSO_4$ pellets) were obtained with a Varian Cary 500 UV–vis NIR spectrometer. Fluorescence spectra were performed on a Hitachi F-4500 fluorescence/phosphorescence spectrophotometer with a 450-W xenon lamp as the excitation source. Electrochemical measurements were performed with a CHI660 electrochemical workstation. A conventional three-electrode system was used. The working electrode was a carbon paste electrode (CPE), a Pt wire as the counter electrode and Ag/AgCl (3 M KCl) electrode was used as a reference electrode.

2.2. *Synthesis*

Compound **1** was prepared by the hydrothermal method: A mixture of $Na_2MoO_4{\cdot}2H_2O$ (1.25 g, 5.17 mM), $MnCl_2{\cdot}2H_2O$ (0.25 g, 1.55 mM), 0.5 mL H_3PO_4, biimidazole (0.268 g, 1.97 mM), and H_2O (18 mL) was stirred for 2 h in air until it was homogeneous. After the pH of the mixture was adjusted to 3.5 with 1 M HCl, the solution was transferred and sealed in a 30 mL Teflon-lined stainless steel autoclave, which was heated at 160 °C under autogenous pressure for five days. The light yellow cubic crystals were isolated and collected by filtration, washed thoroughly with distilled water, and dried at room temperature (53% yield based on Mo). Elemental analysis for $C_{30}H_{66}Mn_2Mo_{10}N_{20}Na_2O_{61}P_4$ (2279.13): Calcd (%): Mn, 4.82; Mo, 42.10; Na, 2.02; C, 15.81; N, 12.29; P, 5.44; H, 2.92. Found: Mn, 4.86; Mo, 42.05; Na, 2.07; C, 15.76; N, 12.33; P, 5.41; H, 2.90.

2.3. *Preparation of 1-CPEs*

Compound **1**-modified carbon paste electrode (**1**-CPEs) was fabricated as follows: 300 mg of graphite powder and 30 mg of complex were mixed and ground together by agate mortar and pestle to achieve a uniform mixture. To the mixture, three drops of Nujol were added with stirring. The homogenized mixture was packed into a glass tube with 1.2 mm inner diameter, and the tube surface was wiped with paper. Electrical contact was established with a copper rod through the back of the electrode.

2.4. *X-ray crystallography*

The crystal structure of **1** was determined from single crystal X-ray diffraction data. Intensity data were collected on a Bruker SMART CCD diffractometer equipped with graphite monochromated Mo Kα radiation (k = 0.71073 Å). The structure was solved by direct methods and difference Fourier map with SHELXL-97 program [21], and refined by full-matrix least-squares techniques on F^2. For **1**, all non-hydrogen atoms except solvent water were refined anisotropically. The positions of hydrogens of organic molecules were calculated theoretically, and refined using a riding model. Hydrogens of water molecules were not treated. Graphics were obtained with Diamond [22]. The crystal parameters, data collection, and refinement results for the compound are summarized in table 1. Selected bond lengths and angles for **1** are listed in table (S1, see online supplementary material at http://dx.doi.org/10.1080/00958972.2014.946414).

Table 1. Crystal data and structure refinement details for **1**.

Empirical formula	$C_{30}H_{66}Mn_2Mo_{10}N_{20}Na_2O_{61}P_4$
M	2922.17
λ (Å)	0.71073
T (K)	273(2)
Crystal dimensions/mm	0.34 × 0.32 × 0.26
Crystal system	Triclinic
Space group	*P-1*
Unit-cell dimensions	a = 11.1994(9)
	b = 11.2440(9)
	c = 20.5567(16)
	α = 97.2980(10)
	β = 91.1190(10)
	γ = 116.9960(10)
V (Å^3)	2279.1(3)
Z	1
D_{Calcd}(Mg m^{-3})	2.129
μ (mm^{-1})	4.641
F (0 0 0)	1426
θ Range (°)	2.36–28.40
Measured reflections	18,562
Independent reflections	10,968
Data/restraints/parameters	10,968/0/616
R_{int}	0.0206
R_1 ($I > 2\sigma(I)$)[a]	0.0355
wR_2 (all data)[a]	0.1063
Goodness-of-fit on F^2	1.054
$\Delta\rho_{max,\ min}$ (e Å^{-3})	1.307/−0.680

[a]$R_1 = \sum||F_0| - |F_C||/\sum|F_0|$; $wR_2 = \sum[w(F_0^2 - F_C^2)^2]/\sum[w(F_0^2)^2]^{1/2}$.

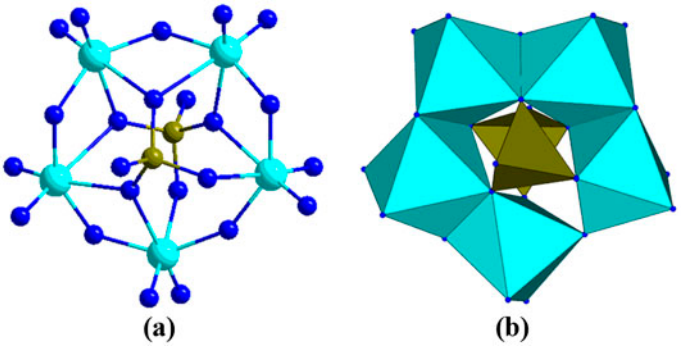

Figure 1. (a) Ball and stick representation for the basic building unit of $[P_2Mo_5O_{23}]^{6-}$ and (b) its polyhedral representation.

3. Results and discussion

3.1. *Crystal structure*

Single crystal X-ray structural analysis reveals that **1** was based on biphosphopentamolybdate. As shown in figure 1, the $[P_2Mo_5O_{23}]^{6-}$ cluster can be described as a ring of five MoO_6 octahedra with two PO_4 tetrahedra capping. Five distorted MoO_6 octahedra generate

a pentagonal ring by sharing edges and corners, and two PO_4 tetrahedra connect to each side of the ring, sharing three oxygens with different MoO_6 units. All the P–O and Mo–O distances are in the normal ranges.

Bond-valence sum (BVS) calculations [23] show 6.02–6.05 for all molybdenum ions and 4.92–4.96 for all phosphorus ions in **1**, indicating that all Mo are +6 and P are +5. BVS calculations are from 1.25 to 1.27 for the protons of the phosphato groups and 0.79–0.92 for hydroxyl groups linked to Mn centers. The terminal water ligands linked to Mn and Na centers (0.26–0.34) are also determined by the BVS calculations. The Mn and Na are +2 and +1 oxidation states, respectively, in **1**.

The basic unit of **1** contains two $[P_2Mo_5O_{23}]^{6-}$ clusters, one $[\{Na_{0.5}(H_2O)_{0.5}\}_2\{Mn(OH)_4(H_2O)_2\}\{Na_{0.5}(H_2bim)\}_2]$ pentanuclear segment, one $\{Mn(H_2O)_4\}$ linker, three protonated H_2bim ligands, and four lattice waters (see figure S1). In **1**, there are two crystallographically independent manganese ions which adopt octahedral coordination geometry. Mn(2) exhibits a distorted $\{MnO_6\}$ octahedral geometry surrounded by two oxygens from two adjacent $[P_2Mo_5]$ clusters and four from water molecules with Mn(2)–O bond distances of 2.167(3)–2.172(4) Å. In the pentanuclear unit $[\{Na_{0.5}(H_2O)_{0.5}\}_2\{Mn(OH)_4(H_2O)_2\}\{Na_{0.5}(H_2bim)\}_2]$, the central Mn(1) ion also adopts distorted $\{MnO_6\}$ octahedral geometry surrounded by four μ–O from adjacent Na cations, and two waters with Mn(1)–O bond distances of 2.178(4)–2.186(4) Å. The sodium cations are half-occupied and exhibit two kinds of coordination geometries. Na(1) cations adopt rare distorted trigonal bipyramid coordination environment [24] with one μ–O from central Mn, three oxygens from $\{MoO_6\}$ octahedra of adjacent $\{P_2Mo_5\}$ clusters, and a nitrogen from bim. Na(2) cation has a distorted tetrahedral center with one μ–O from central Mn, two oxygens from $\{MoO_6\}$ octahedra of $\{P_2Mo_5\}$ clusters, and one water. The Na–N distance is 2.950 Å and the Na–O distances vary from 2.664 to 2.826 Å. In this linkage mode, four Na ions, one Mn center, and two bim ligands are bonded together by four μ–O bridges to form unusual pentanuclear fragments $[\{Na_{0.5}(H_2O)_{0.5}\}_2\{Mn(OH)_4(H_2O)_2\}\{Na_{0.5}(H_2bim)\}_2]$ (figure 2). Each pentanuclear segment links four adjacent Standberg units to form infinite supramolecular dimer chains. These dimer chains are parallel with each other and further connected by $Mn(H_2O)_4$ linkers to yield unique 2-D layer (see figure 3). Two different types of cage-like pores are observed in alternating type along the crystallographic *b* axis. Two $\{P_2Mo_5O_{23}\}$ clusters and two pentanuclear fragments $[\{Na_{0.5}(H_2O)_{0.5}\}_2\{Mn(OH)_4(H_2O)_2\}\{Na_{0.5}(H_2bim)\}_2]$ are connected alternately to form pore A, which is filled by protonated H_2bim ligands (see figure 3). The bigger pore B is formed by four $\{P_2Mo_5O_{23}\}$ cages, two $Mn(H_2O)_4$ units,

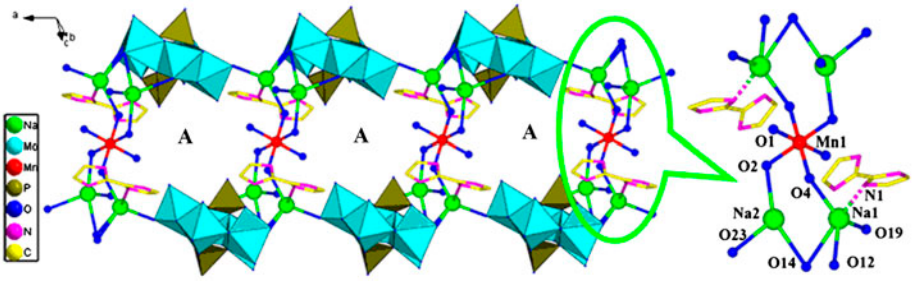

Figure 2. The 1-D dimer chain of the poly(oxo molybdophosphate) based on $[P_2Mo_5]$ and pentanuclear $[\{Na_{0.5}(H_2O)_{0.5}\}_2\{Mn(OH)_4(H_2O)_2\}\{Na_{0.5}(H_2bim)\}_2]$ linkers in **1**.

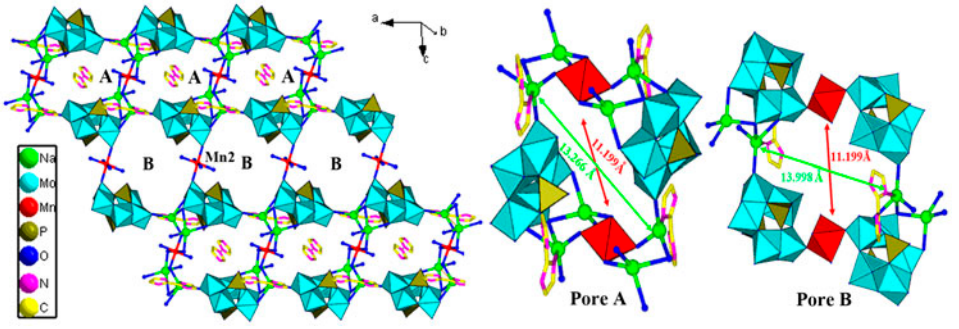

Figure 3. The 2-D layer of **1** connected by $Mn(H_2O)_4$ linkers and the linkage detail and dimension of the A and B holes.

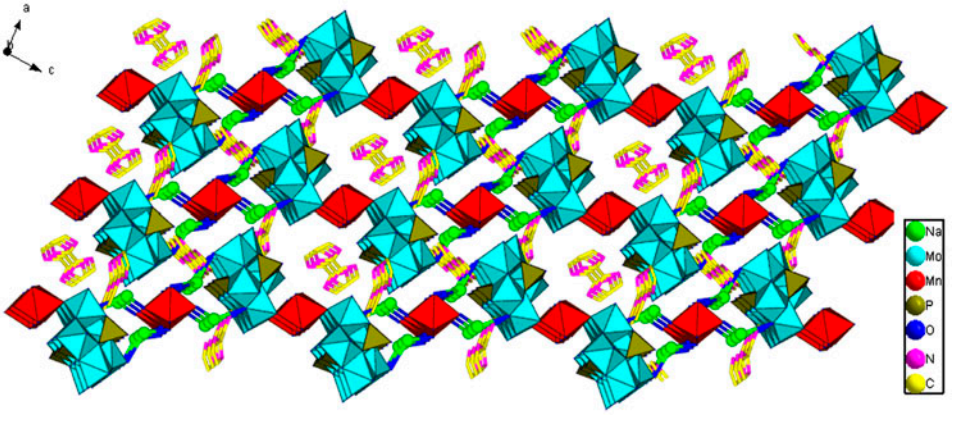

Figure 4. View of the 3-D framework of **1** constructed by π–π stacking interactions forming a 2-D plane.

and two Na(bim) fragments (see figure 3). The dimension of pore A is 11.199 × 13.266 Å with Mn(1)–Mn(1) distance of 11.199 Å and Na(1)–Na(1) distance 13.266 Å. The dimension of pore B is 11.199 × 13.998 Å with Mn(2)–Mn(2) distance 11.199 Å, Na(1)–Na(1) distance is 13.998 Å. In the packing arrangement, the adjacent 2-D layers are further linked to form a 3-D structure by π–π interactions between aromatic groups of bim ligands (figure 4 and figure S2).

3.2. *Spectroscopic and thermal analyses*

3.2.1. IR spectrum. IR spectrum of **1** was measured at room temperature (shown in figure S3). The broad bands at 3431 and 3153 cm^{-1} can be assigned to ν(N–H) and/or ν(O–H) of the protonated ligands and isolated solvent water molecules. The peaks at 1032, 909, 778, and 687 cm^{-1} are attributed to ν(P–O), ν(Mo = Od), ν(Mo–Ob–Mo), and ν(Mo–Oc–Mo), respectively, of the P_2Mo_5 polyanions. Absorption peaks at 1209–1645 cm^{-1} are associated with ν(C–N) vibrations of bim ligands.

3.2.2. Powder X-ray diffraction analysis. The simulated and experimental Powder X-ray diffraction patterns of **1** are presented in figure S4. The diffraction peaks of both simulated and experimental patterns match in the key positions, indicating the phase purity of **1**. The difference in intensity may be due to the preferred orientation of the powder samples.

3.2.3. TG analysis. In the TG curve of **1** (see figure S5), the first weight loss of 8.51% from 100 to 170 °C corresponds to release of water, in accordance with the calculated value of 8.06% ($13H_2O$). The second weight loss of 23.34% from 273 to 386 °C is attributed to the loss of all biimidazole organic ligands, which is close to the calculated value of 23.07% (~5 bim). The third weight loss of 19.23% from 470 to 700 °C is ascribed to the release of P_2O_5. The weight losses from the TG curves are consistent with the molecular formula of **1**.

3.2.4. UV spectrum. The UV–vis absorption spectrum of **1** is shown in figure S6. Absorptions at 237 and 296 nm are attributed to (LMCT) $p\pi$ ($O_{terminal}$)$\rightarrow d\pi^*$ (Mo) electronic transitions in the Mo=O bonds and $d\pi$–$p\pi$–$d\pi$ electronic transitions between the energy levels of the Mo–O–Mo bonds [25].

3.3. *Fluorescent properties*

The fluorescence spectrum of **1** in the solid state at room temperature is shown in figure 5. Compound **1** exhibited fluorescence with an emission maximum at 454 nm upon excitation at 382 nm. The small red shifts compared to that of free bim (emission maximum at ca. 436 nm upon excitation at ca. 335 nm [26]) may be a combination of several factors [27] including the LMCT emission [28] and a change in the highest occupied molecular

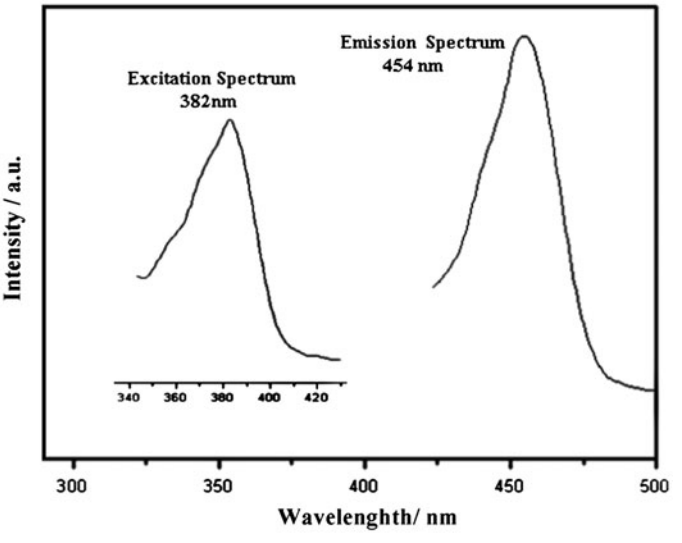

Figure 5. Fluorescence spectra of **1** in the solid state at room temperature.

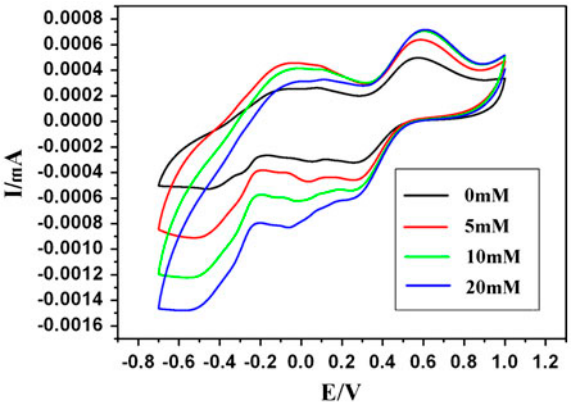

Figure 6. Cyclic voltammograms of **1**-CPE in 1 M H_2SO_4 solution containing hydrogen peroxide at different concentrations (potentials *vs.* SCE. Scan rate: 50 mV s^{-1}).

orbital and lowest unoccupied molecular orbital energy levels of intraligand emission from the protonated ligands [29]. The results indicate that **1** is a potential fluorescence-emitting material.

3.4. *Electrochemical and electrocatalysis properties*

The cyclic voltammetric behavior of modified carbon paste electrode for **1** (**1**-CPE) in 1 M H_2SO_4 aqueous solution was recorded at different scan rates from 1.0 to −0.8 V (figure S7). There exist three reversible redox peaks with half-wave potentials $E_{1/2} = (E_{pa} + E_{pc})/2$ at I-I′ (+421 mv), II-II′ (+181 mv), and III-III′ (+480mv) (based on 50 mV s^{-1}), ascribed to three consecutive two-electron processes of Mo [18, 19]. However, the expected oxidation peak of Mn centers is not observed, perhaps due to overlap with the Mo^{VI}/Mo^{V} redox peak. When scan rates varied from 50 to 290 mV s^{-1}, the peak potentials change gradually with the cathodic peak potentials shifting to the negative direction and the corresponding anodic peak potentials to the positive direction with increasing scan rates. Furthermore, **1**-CPE displays good electrocatalytic activity on reduction of hydrogen peroxide (figure 6). At the **1**-CPE, with the addition of H_2O_2, all three reduction peak currents increased, while the corresponding oxidation peak currents dramatically decreased, suggesting that H_2O_2 was reduced by all three reduced polyoxoanion species.

4. Conclusion

Mn^{2+} and unusual pentanuclear fragments are introduced into $\{P_2Mo_5\}$ system to yield an infinite 2-D supramolecular layer with two cage-like pores. The fluorescence and the electrocatalytic activity of **1** are reported. Further work on the introduction of other metal ions as well as organonitrogen ligands into $\{P_2Mo_5\}$ hybrids is under way.

Supplementary material

CCDC 981689 contains the supplementary crystallographic data for this article. These data can be obtained free of charge from The Cambridge Crystallographic Data Center via www.ccdc.cam.ac.uk/data_request/cif. Supplementary data associated with this article can be found in the online version.

Funding

This work was supported the National Natural Science Foundation of China [grant number 21271056] and [grant number 21371042]; the Ministry of Education and Specialized Research Fund for the Doctoral Program of Higher Education [grant number 20122329110001]; the Natural Science Foundation of Heilongjiang Province [grant number B201216], Key Laboratory of Functional Inorganic Material Chemistry (Heilongjiang University), Ministry of Education, Doctoral initiation Foundation of Harbin Normal University [grant number KGB201214]; Program for Scientific and Technological Innovation Team Construction in Universities of Heilongjiang Province [grant number 2011TD010].

References

[1] A. Müller, H. Reuter, S. Dillinger. *Angew. Chem. Int. Ed Engl.*, **34**, 2328 (1995).
[2] M.T. Pope, A. Müller. *Angew. Chem. Int. Ed Engl.*, **30**, 34 (1991).
[3] X.L. Wang, C. Qin, E.B. Wang, Z.M. Su, L. Xu. *Angew. Chem. Int. Ed.*, **43**, 5036 (2004).
[4] S.L. Zheng, J.H. Yang, X.L. Yu, X.M. Chen, W.T. Wong. *Inorg. Chem.*, **43**, 830 (2004).
[5] H. Zhang, L.Y. Duan, Y. Lan, E.B. Wang. *Inorg. Chem.*, **42**, 8053 (2003).
[6] D.W. Zhou, H. Zhang, Z.F. Yang. *Chin. J. Struct. Chem.*, **25**, 312 (2006).
[7] X.M. Li, Y.G. Chen, C.N. Su, S. Zhou, Q. Tang, T. Shi. *Inorg. Chem.*, **52**, 11422 (2013).
[8] J. Thomas, A. Ramanan. *Cryst. Growth Des.*, **8**, 3390 (2008).
[9] K. Yu, B.B. Zhou, Y. Yu, Z.H. Su, C.M. Wang, C.X. Wang, S. Gao. *Inorg. Chim. Acta*, **384**, 8 (2012).
[10] B.S. Zhang, C.S. Wu, J.P. Qiu, Y.X. Li, Z.X. Liu. *J. Coord. Chem.*, **67**, 787 (2014).
[11] Y. Yu, K. Yu, B.B. Zhou, Z.F. Zhao, Z.H. Su. *Chin. J. Struct. Chem.*, **29**, 1505 (2010).
[12] W. Wang, Y.F. Qiu, L. Xu. *J. Coord. Chem.*, **67**, 797 (2014).
[13] Y. Wang, L. Ye, T.G. Wang, X.B. Cui, S.Y. Shi, G.W. Wang, J.Q. Xu. *Dalton Trans.* 1916 (2010).
[14] L.-M. Wang, H.-Y. Guo, S. Li, Y.-Y. Hu, Y. Wang, L.-N. Xiao, D.-C. Zhao, Z.-M. Gao, D.-F. Zheng, X.-B. Cui, Y. Fan, J.-Q. Xu. *J. Coord. Chem.*, **67**, 728 (2014).
[15] Y. Ding, J.X. Meng, W.L. Chen, E.B. Wang. *CrystEngComm*, **13**, 2687 (2011).
[16] Y. Wang, L.C. Zhang, Z.M. Zhu, N. Li, A.F. Deng, S.Y. Zheng. *Transition Met. Chem.*, **36**, 261 (2011).
[17] G.C. Ou, X.Y. Yuan, Z.Z. Li, M.H. Ding. *J. Coord. Chem.*, **66**, 2065 (2013).
[18] H.J. Jin, B.B. Zhou, Y. Yu, Z.F. Zhao, Z.H. Su. *CrystEngComm*, **13**, 585 (2011).
[19] L. Song, K. Yu, Z.H. Su, C.X. Wang, C.M. Wang, B.B. Zhou. *J. Coord. Chem.*, **67**, 522 (2014).
[20] K. Yu, B.-B. Zhou, Y. Yu, Z.-H. Su, H.-Y. Wang, C.-M. Wang, C.-X. Wang. *Dalton Trans.*, **41**, 10014 (2012).
[21] G.M. Sheldrick. *SHELXL 97, Program for Crystal Structure Refinement*, University of Gőttingen, Germany (1997).
[22] K. Brandenburg, *Diamond (Version 3.1e), Crystal and Molecular Structure Visualization, Crystal Impact*, Brandenburg, K. & Putz Gbr, H., Bonn, Germany (2007).
[23] D. Brown, D. Altermatt. *Acta Crystallogr.*, **41**, 244 (1985).
[24] Y. Zhang, J.Q. Shen, L.H. Zheng, Z.M. Zhang, E.B. Wang. *Cryst. Growth Des.*, **14**, 110 (2014).
[25] M.T. Pope. *Heteropoly and Isopoly Oxometalates*, Springer-Verlag, Berlin (1983).
[26] Z.Q. Hu, X.Z. Ye, X.G. Song, S.M.L. Inorg. *Chem.*, **27**, 1993 (2011).
[27] S.L. Li, Y.Q. Lan, J.F. Ma, J. Yang, G.H. Wei, L.P. Zhang, Z.M. Su. *Cryst. Growth Des.*, **8**, 675 (2008).
[28] K. Yu, B. Wan, Y. Yu, L. Wang, Z.H. Su, C.M. Wang, C.X. Wang, B.B. Zhou. *Inorg. Chem.*, **52**, 485 (2013).
[29] M.L. Qi, K. Yu, Z.H. Su, C.X. Wang, C.M. Wang, B.B. Zhou, C.C. Zhu. *Inorg. Chim. Acta*, **400**, 59 (2013).